Amplified Stimulated Terahertz Emission at Room temperature from Optically Pumped Graphene

Stephane Boubanga Tombet,[*,†,‖] Silvia Chan,[†,‡] Taiichi Otsuji,[†,¶] Akira Satou,[†,¶] and Victor Ryzhii[§,¶]

Research Institute of Electrical Communication, Tohoku University, Sendai, Japan, NanoJapan Program, Rice University and Department of Materials Science and Engineering, USA, JST-CREST, Chiyoda-ku, Tokyo, Japan, and University of Aizu, Aizu-Wakamatsu, Fukushima, Japan

E-mail: stephanealbon@hotmail.com

Phone: +81-22-217-6104. Fax: +81-22-217-6104

Abstract

Room temperature Terahertz stimulated emission and population inversion in optically pumped graphene is reported. We experimentally observe fast relaxation and relatively slow recombination dynamics of photogenerated electrons/holes in an exfoliated graphene on SiO_2/Si substrate under pumping with a 1550-nm, 80-fs pulsed fiber laser beam and probing with the corresponding terahertz beam generated by optical rectification in a nonlinear electro optical sensor. The time-resolved electric-field intensity originating from the coherent terahertz

[*]To whom correspondence should be addressed
[†]Tohoku University
[‡]University of Pennsylvania
[¶]JST-CREST
[§]University of Aizu
[‖]Current address: 2-1-1 Katahira, Aoba-ku, Sendai, Miyagi 980-8577, Japan

photon emission is electro-optically sampled in an total-reflection geometry. The comparison of terahertz electric fields intensities measured on SiO_2/Si substrate and that one from graphene clearly indicate that graphene sheet act like an amplifying medium. The Emission spectra agrees relatively well the pumping photon spectrum and its dependency on the pumping power shows a threshold like behavior, testifying the occurrence of the negative conductivity in the THz spectral range and the population inversion. The threshold pumping intensity > $5 * 10^6 W/cm^2$ is in a good agreement with simulations.

Introduction

Graphene is a one-atom-thick planar sheet of carbon atoms that are densely packed in a honeycomb crystal lattice.[1] The fabrication of graphene overthrows the prediction that strictly two-dimensional crystal cannot exist in finite temperature because of thermal disturbance.[2] graphene has many peculiar properties and potential applications. For example, the prediction and observation of half-integer quantum hall effect,[3] finite conductivity at zero charge carrier concentration,[4] perfect quantum tunneling effect,[5] ultrahigh carrier mobility,[6] including massless and gapless energy spectra. The gapless and linear energy spectra of electrons and holes lead to nontrivial features such as negative dynamic conductivity in the terahertz (THz) spectral range,[7] which may lead to the development of a new type of THz laser.[8,9]

The optical conductance of graphene based systems in the THz to far infrared regime has been a topic of intense interest due to the ongoing search for viable THz detectors and emitters. A series of work searching for application of graphene in THz science and technology have been carried out and suggest that graphene can be used in building innovative devices for THz optoelectronics.

To realize such THz graphene-based devices, understanding the non-equilibrium carrier relaxation/recombination dynamics is critical. [figure][1][]1 presents the carrier relaxation/recombination processes and the non-equilibrium energy distributions of photoelectrons/photoholes in optically pumped graphene at specific times from $\sim$ 10 fs to picoseconds after pumping. It is known that photoexcited carriers are first cooled and thermalized mainly by intraband relaxation processes on

femtosecond to subpicosecond time scales, and then by interband recombination processes. Recently, time-resolved measurements of fast non-equilibrium carrier relaxation dynamics have been carried out for multilayers and monolayers of graphene that were epitaxially grown on SiC[10–14] and exfoliated from highly oriented pyrolytic graphite (HOPG).[15,16] Several methods for observing the relaxation processes have been reported. Dawlaty et al.[10] and Sun et al.[11] used an optical-pump/optical-probe technique and George et al.[12] used an optical-pump/THz-probe technique to evaluate the dynamics starting with the main contribution of carrier-carrier (cc) scattering in the first 150 fs, followed by observation of carrier-phonon (cp) scattering on the picosecond time scale. Ultrafast scattering of photoexcited carriers by optical phonons has been theoretically predicted by Ando,[17] Suzuura[18] and Rana.[19] Kamprath et al.[15] observed strongly coupled optical phonons in the ultrafast carrier dynamics for a duration of 500 fs by optical-pump/THz-probe spectroscopy. Wang et al.[14] also observed ultrafast carrier relaxation via emissions from hot-optical phonons for a duration of $\sim$ 500 fs by using an optical-pump/optical-probe technique. The measured optical phonon lifetimes found in these studies were $\sim$ 7 ps,[15] 2-2.5 ps,[14] and $\sim$ 1 ps,[12] respectively, some of which agreed fairly well with theoretical calculations by Bonini et al.[20] A recent study by Breusing et al.[16] more precisely revealed ultrafast carrier dynamics with a time resolution of 10 fs for exfoliated graphene and graphite.

In this paper we report on the fast relaxation and relatively slow recombination dynamics of optically-pumped and THz-probed exfoliated graphene on SiO_2/Si substrate. The results reflect the recombination of photoelectrons and photoholes after the intraband ultrafast carrier relaxation, and suggest the occurrence of negative dynamic conductivity in the THz spectral range.

Dynamic Conductivity of Optically Pumped Graphene

First we consider the case of cold electronic temperature conditions (such like cryogenic temperature environment with weak optical pumping). It has been shown that the intraband carrier equilibration in optically excited graphene (with pumping photon energy $\hbar\Omega$) first establishes sep-

arate quasi-equilibrium distributions of electrons and holes at around the level $\varepsilon_f \pm \hbar\Omega/2$ (ε_f : Fermi energy) within 20-30 fs after excitation (see [figure][1][]1b), followed by cooling of these electrons and holes mainly by emission of a cascade (N times) of optical phonons ($\hbar\omega_0$) within 200-300 fs to occupy the states $\varepsilon_f \pm \varepsilon_N \approx \hbar(\Omega/2 - N\omega_0)$, $\varepsilon_N < \hbar\omega_0$ (see [figure][1][]1c upper). Then, thermalization occurs via electron-hole recombination as well as intraband Fermization due to cc scattering and cp scattering (as shown with energy $\hbar\omega_q$ in [figure][1][]1a) on a few picoseconds time scale (see [figure][1][]1d upper), while the interband cc scattering and cp scattering are slowed by the density of states effects and Pauli blocking.

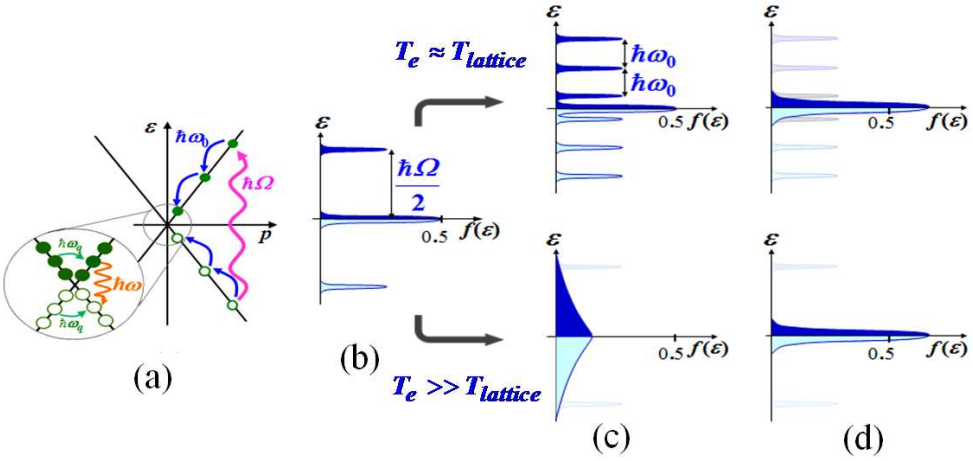

Figure 1: Schematic view of graphene band structure (a) and energy distributions of photogenerated electrons and holes (b)-(d). Arrows denote transitions corresponding to optical excitation by photons with energy $\hbar\Omega$ cascade emission of optical phonons with energy $\hbar\omega_0$ and radiative recombination with emission of photons with energy $\hbar\omega$. (b) after $\sim$ 20 fs from optical pumping, (c) after 200$\sim$300 fs from optical pumping, upper: phonon-cascade-emission dominant case, lower: cc-scattering-dominant case for high electronic temperature, (d) after a few ps from optical pumping, upper: phonon-cascade-emission dominant case, lower: cc-scattering-dominant case for high electronic temperature.

When the photogenerated electrons and holes are heated for the case of room temperature environment and/or strong pumping, collective excitations due to the cc scattering, e.g., intraband plasmons should have a strong influence on the carrier relaxation dynamics. As is discussed in [12,15,16] the initial distribution shown in [figure][1][]1b rapidly thermalizes and cools via the cc scattering (see [figure][1][]1c lower). Hence, there are no cascade emissions of optical phonons but optical phonons are emitted by carriers on the high-energy tail of the electron and hole distributions (see

[figure][1][]1d lower).

For the electron-hole recombination, radiative recombination via direct-transition to emit photons $\hbar\omega \approx \varepsilon_N$ and non-radiative recombination via Auger processes, plasmon emissions, and phonon emissions[12,21] are considered. In the case of the radiative recombination, due to the relatively small values of $\hbar\omega \approx \varepsilon_N < \hbar\omega_0$ as well as the gapless symmetrical band structure, photon emissions over a wide THz frequency range are expected if the pumping photon energy is suitably chosen and the pumping intensity is sufficiently high. In the cold electronic temperature conditions case the incident photon spectra are expected to be reflected in the THz photoemission spectra as evidence that such a process occurs.

In this work, we observed amplified stimulated THz emission at room temperature from optically pumped and THz-probed graphene on SiO_2/Si substrate and verified the occurrence of negative dynamic conductivity.

At room temperature, the thermal carrier concentration reaches $10^{11} cm^{-2}$ and upon strong pumping the cc scattering is frequent enough to broaden the absorption spectrum of the pumping light so that it might even thermalize the carriers before the optical phonon (OP) emissions. Let us consider that case in which carriers are thermalized by the cc scattering. For this cc-scattering case where the cc scattering is dominant and carriers which are always in a quasi-equilibrium suffer energy relaxation and recombination via the OP scattering (latter only via interband OPs), we can assume the carrier distribution as $f_\Xi = 1/\left\{1 + exp()\left[\left(\Xi - \varepsilon_f\right)/k_B T_e\right]\right\}$ where ε_f is the quasi-Fermi energy for carriers and T_e is the carrier temperature. Under optical pumping with photon energy $\hbar\Omega$ the carrier distribution (equivalent electron and hole distributions) is governed by the balance equations for the total energy and concentration of carriers[18,19]

$$\frac{\mathrm{d}}{\mathrm{d}t}\Sigma = \frac{1}{\pi^2}\sum_{i=\Gamma,K}\int dk\left[\frac{1}{\tau^{(+)}_{i,inter}}(1 - f_{\hbar\omega_i - v_w\hbar k})(1 - f_{v_w\hbar k}) - \frac{1}{\tau^{(-)}_{i,inter}} f_{\hbar\omega_i - v_w\hbar k} f_{v_w\hbar k}\right] \qquad (1)$$

$$\frac{\mathrm{d}}{\mathrm{d}t}\Xi = \frac{1}{\pi^2}\sum_{i=\Gamma,K}\left\{\int dk v_w \hbar k\left[\frac{1}{\tau^{(+)}_{i,inter}}(1-f_{\hbar\omega_i - v_w\hbar k})(1-f_{v_w\hbar k}) - \frac{1}{\tau^{(-)}_{i,inter}} f_{\hbar\omega_i - v_w\hbar k} f_{v_w\hbar k}\right]\right.$$
$$\left. + \int dk \hbar\omega_i f_{v_w\hbar k}\left[\frac{1}{\tau^{(+)}_{i,intra}}(1-f_{\hbar\omega_i + v_w\hbar k}) - \frac{1}{\tau^{(-)}_{i,intra}}(1-f_{\hbar\omega_i - v_w\hbar k})\right]\right\} \quad (2)$$

Where $n(\varepsilon_f(t), T_e(t))$ and $\Xi(\varepsilon_f(t), T_e(t))$ are carrier concentration and energy density, $\tau^{(\pm)}_{i,inter}$ and $\tau^{(\pm)}_{i,intra}$ are relaxation times for interband and intraband optical phonon ("+" for absorption and "-" for emission; i = Γ, K).

[figure][2][]2 shows the carrier temperature and quasi-Fermi energy resulting from the calculation of equations (1) and (2). The initial conditions for these equations are just the sum of thermal part and photogenerated part of carrier concentration and energy density: $n(\varepsilon_f(0), T_e(0)) = n_0 + \delta n$ and $\Xi(\varepsilon_f(0), T_e(0)) = \Xi_0 + \delta\Xi$ where $\delta n = (2\pi/\sqrt{\varepsilon})(\alpha I_{pump}/\hbar\Omega)\delta t$ is the photogenerated carrier concentration and $\delta\Xi = (2\pi/\sqrt{\varepsilon})(\alpha I_{pump}/\hbar\Omega)(\hbar\Omega/2)\delta t$ the photogenerated carrier energy. I_{pump} is the peak pulse intensity, $\hbar\Omega$ is the photon energy and δt is the pulse width.

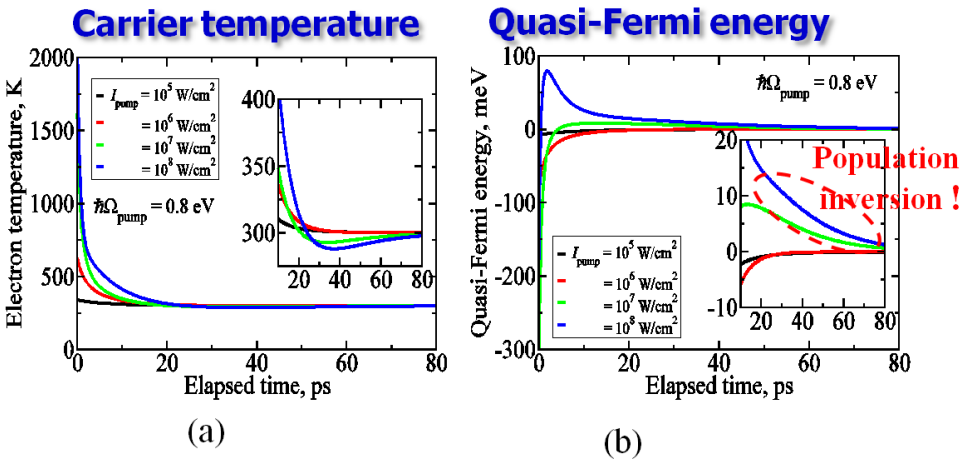

Figure 2: Calculated carrier temperature (a) and quasi-Fermi energy (b) for different values of the pumping pulse intensity for the pumping photon energy of 800 meV using balance equations (1) and (2).

[figure][2][]2a shows the calculated electron temperature under the pumping photon energy of

800 meV for different values of the pumping peak pulse intensity. One can notice from these calculations that, at the beginning after the pulse excitation (optical pumping), the carrier temperature becomes very high ($T_e \sim 2000K$ for $I_{pump} = 10^8 W/cm^2$ and $\hbar\Omega$ = 800 meV) following by a cooling of these electron.

[figure][2][]2b shows the calculated quasi-Fermi energy under the pumping photon energy of 800 meV for different values of the pumping peak pulse intensity. It is clearly seen that, as the electron temperature increases the quasi-Fermi energy becomes negative. However, after a few ps, the quasi-Fermi energy becomes positive and lasts for a few ten ps. These results show that the population inversion ($\varepsilon_f > 0$) can occur at room temperature. The population inversion here occurs due to the imbalance between energy relaxation by intraband optical phonons and recombination by interband optical phonons. The interband optical phonon emission is slower because the most fraction of the interband transition is forbidden by the Pauli Exclusion Principle due to the high energy of optical phonons. This population inversion occurs when the pumping peak pulse intensity exceed $10^6 W/cm^2$.

Samples, Experiments and Results

Samples and experimental setup

In order to verify the proposed concept, we conduct experimental studies on the electromagnetic radiation emitted from an optically pumped graphene structure. The sample used in this experiment is commercial exfoliated graphene on SiO_2/Si substrate . The sample structure as presented in [figure][3][]3 in made of one layer of Si substrate and an thermal dry SiO_2 of 300 nm of thikness. The Si substrate is <100> oriented with about 500-560 μm thickness and 10^{-3}- $5 * 10^{-3}$ Ωcm of resistivity. For the experiments we used a THz time-domain spectroscopy set up based on an optical pump/THz-and-optical-probe technique. The time-resolved field emission properties are measured by an electro-optic sampling method in total-reflection geometry.[22] To obtain the THz photon emissions from the above-mentioned carrier relaxation/recombination dynamics, the

pumping photon energy (wavelength) is carefully selected to be around 800 meV (1550 nm). A femtosecond pulsed fiber laser with full width at half-maximum (FWHM) of 80 fs, and frequency of 20 MHz was used as the pumping source. The graphene sample was placed on the stage and a CdTe crystal of around 120 μm of thickness (100)-oriented and was placed on the sample; the CdTe crystal acts as a THz probe pulse emitter as well as an electro-optic sensor. The single femtosecond fiber laser beam is split into two beams: one for optical pumping and generating the THz probe beam, and one for optical probing. The pumping laser, which is linearly polarized and mechanically chopped at $\sim 1.2KHz$, is simultaneously focused at normal incidence onto the sample and the CdTe from below, while the probing laser, which is cross-polarized to the pumping beam, is focused from above. Owing to second-order nonlinear optical effects, the CdTe crystal can rectify the pumping laser pulse to emit THz envelope radiation. This THz pulse irradiate the graphene sample, acting as THz probe signals to stimulate THz photon emission via electron-hole recombination in the graphene.

The optical-pumping/THz-probing geometry and these beam propagations are schematically shown in [figure][3][]3. The electric field intensity of the THz radiation is electroopticaly detected at the top surface of the CdTe crystal. Along with the propagation of the optical pump pulse through the CdTe crystal the THz pulse is generated and grows up. The THz pulse being emitted from the CdTe crystal is partially reflected at the top surface of the CdTe then subject back to the graphene, working as the THz probe pulse (shown with arrowed blue line in Fig. 3). The graphene responds to this THz probe pulse radiation giving rise to stimulated THz emission. The total round-trip propagation time of the THz pulse through the CdTe crystal and graphene/ SiO_2 epilayer is $\sim$ 3.5 ps assuming the refractive index of CdTe in the THz frequencies to be 3.75. Therefore the original data of the temporal response that we observe in this experiment consist of the first forward propagating THz pulsation (no interaction with graphene) followed by the double reflected secondary THz pulsation (probing the graphene) around 3.5 ps after the first pulsation.

On the other hand, through the Si prism attached to the CdTe crystal, the optical probing beam is totally reflected back to the lock-in detection block, and its phase information reflecting the

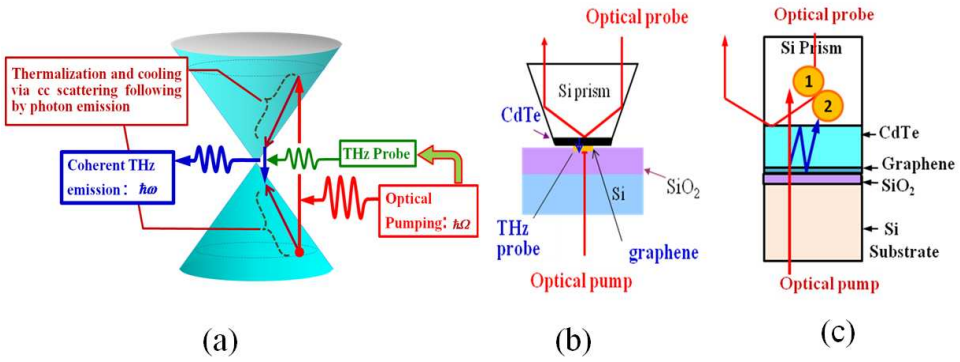

Figure 3: Measurement setup for optical-pump/THz-and-optical-probe spectroscopy. Involved process from optical pumping to emission of stimulated THz photon (a). CdTe crystal on top of the graphene sample, the optical pump and probe as well as the THz probe are represented (b). CdTe crystal generates THz probe which is partially reflected at the top surface of the CdTe then subject back to the graphene. The optical probe allows electro-optic detection of these THz electric field intensities (c).

electric field intensity is lock-in amplified. By sweeping the timing of the optical probe using an optical delay line, the whole temporal profile of the field emission properties can be obtained. The system bandwidth is estimated to be around 6 THz, which is limited mainly by the Reststrahlen band of the CdTe sensor crystal.

Samples and experimental setup

[figure][4][]4 shows temporal responses measured in the EOS set up. On each graphs two different measurements are presented, these measurements was done in the same conditions. The stage with the sample was alternatively moved in order to have the optical pump beam on the SiO_2/Si substrate for one measurement and on the graphene area for the other one without changing the optical pump and probe path. The red curve is the response measured on the SiO_2/Si substrate (without graphene) took as the reference and the black curve is the response obtained on graphene + substrate. Each temporal profile reflect the way the THz incoming electric field at the CdTe top surface changes the phase information of the optical probe beam. Once the optical rectification (OR) generated THz pulse reach the top surface one have the first pulsation presented in [figure][4][]4 (see also the arrowed blue line in [figure][3][]3). This THz field is partially reflected at CdTe upper

surface (at the interface between CdTe and Si prism) and second time at the CdTe back surface (at the interface between CdTe and graphene/SiO_2) , once this second THz pulse reach the top surface one have the second pulsation presented in [figure][4][]4. The measured time delay between these two pulsation of around 3.5 ps is in a quite good agreement with the round trip propagation time of THz pulse through the CdTe crystal and graphene/SiO_2 epilayer.

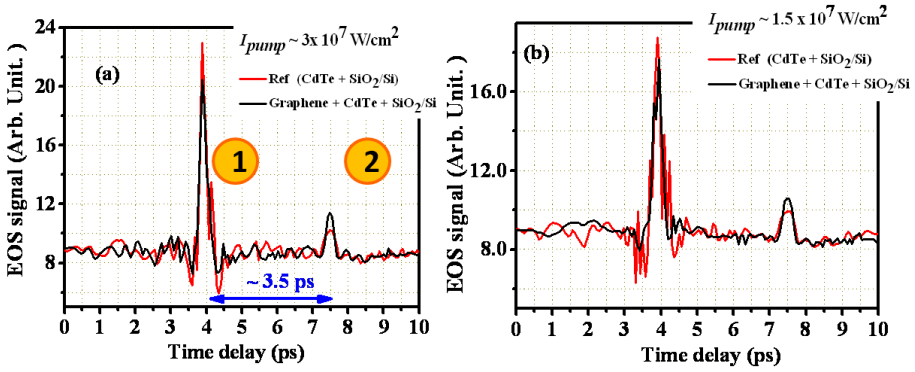

Figure 4: Measured temporal responses on the SiO_2/Si substrate (red lines) and graphene + substrate (black lines) for the pumping pulse intensities of about $3*10^7 W/cm^2$ (a) and $1.5*10^7 W/cm^2$ (b). The grid of the vertical axis for each plot is scaled identically for both "red line" and "black line".

The results presented in [figure][4][]4a was obtained for the pumping pulse intensity of about $3*10^7 W/cm^2$. One can notice on these results that the secondary pulsation measured on graphene + substrate (black curve) is more intense than that one obtained on the SiO_2/Si substrate (black curve), suggesting an amplification phenomena. [figure][4][]4b, present the same measurements for the pumping pulse intensity of about $1.5*10^7 W/cm^2$. One can notice that when reducing I_{pump} , the intensity of the second pulsation coming from graphene + substrate decreases relatively to that one coming from only the substrate.

The emission spectrum from CdTe + SiO_2/Si substrate (without graphene) in [figure][5][]5 shows a dominant peak around around 1 THz, (red line in [figure][5][]5). The blue line present the photoemission spectrum predicted from the pumping laser spectrum in the cold electronic temperature conditions (see the Inset of [figure][5][]5). The black line shows the emission spectrum from CdTe + graphene, this spectrum agree relatively well the THz photon spectrum predicted

from the pumping photon spectrum. We want to stress that the perfect agreement between these spectra is only expected at cryogenic temperature environment with weak optical pumping when the OP scattering is dominant and carriers take a quasi-equilibrium by the cc scattering after the cascade emission of OPs.

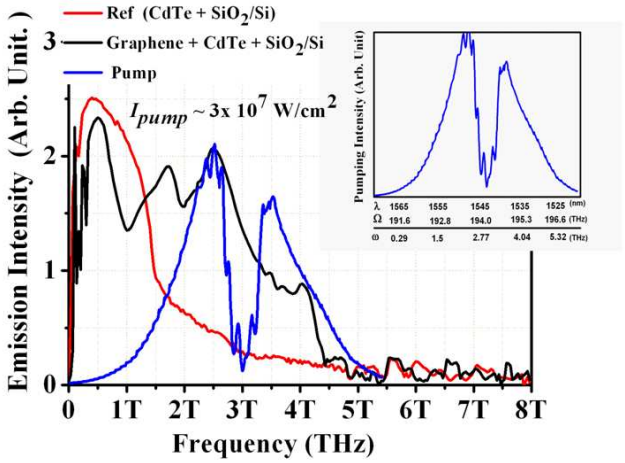

Figure 5: Fourier spectra of the measured temporal response in the case when the pumping pulse intensity of about $3 * 10^7 W/cm^2$ form SiO_2/Si substrate (red line) and graphene + substrate (black line). Blue line is the photoemission spectrum predicted from the pumping laser spectrum in the cold electronic temperature conditions when OP scattering is dominant and carriers take a quasi-equilibrium by the cc scattering after the cascade emission of OPs. The grid of the vertical axis is scaled identically for both "red line" and "black line".

It is thought that the THz emissions from graphene are stimulated by the coherent THz probe radiation that originates from OR in CdTe excited by the pump laser beam. The THz emission is amplified by photoelectron/hole recombination in the range of the negative dynamic conductivity. The ratio of the spectra of the "graphene + CdTe + SiO_2/Si substrate" to that of the "CdTe + SiO_2/Si substrate" corresponds to the transfer function of the graphene sheet.

[figure][6][]6a shows the transfer function of the graphene sheet for different values of pumping pulse intensity. The emission is drastically reduced when decreasing the beam power. One can also notice that below $5 * 10^6 W/cm^2$ the emission completely disappear and only attenuation can be seen.

The [figure][6][]6b show the evaluated grain obtained by deviding the electric field intensity measured on graphene + SiO_2/Si substrate (black curve in [figure][4][]4) by that one measured

only on SiO_2/Si substrate (red curve in [figure][4][]4). A threshold like behavior can be seen testifying the occurrence of the negative conductivity and population inversion in optically pumped graphene. Once this population inversion obtained the graphene sheet act like an amplifying medium. This is a quite promising possibility for the realization of room temperature THz lasers based on graphene.

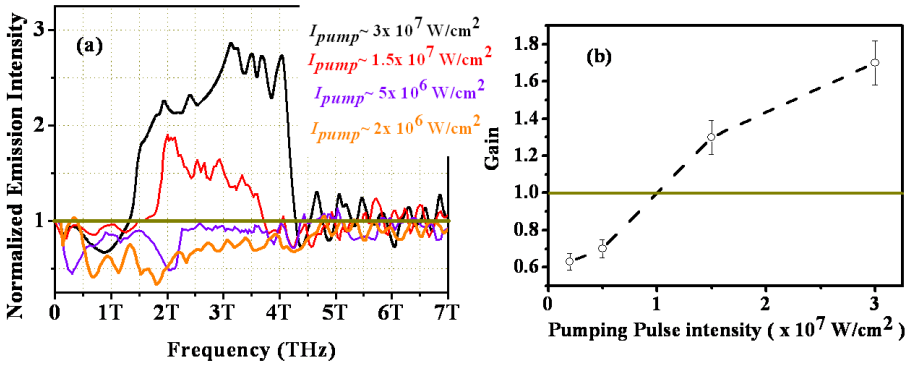

Figure 6: Transfer function of the graphene sheet for different values of pumping pulse intensity (a). Corresponding gain versus the pumping pulse intensity (b)

Furthermore, to confirm the effects of the THz probe that stimulate the emission in graphene, the CdTe crystal have been replaced with another CdTe crystal having a high-reflectivity coating for IR on its bottom surface, in order to eliminate generation of the THz probe signal. In this case, no distinctive response was observed on the SiO_2/Si substrate or on graphene. One should also stress that since the time delay between pulsations (1) and (2) presented in see [figure][4][]4b depend on the CdTe crystal thickness, the crystal have been replaced with another 0.08-mm-thick (110)-oriented CdTe crystal and the time delay of about 2 ps was measured between these pulsation once again in good agreement with the round trip propagation time of THz pulse through the CdTe crystal and graphene/ SiO_2 epilayer.

Since the measurements are taken as an average, the observed response is undoubtedly a coherent process that cannot be obtained via spontaneous emission processes, providing clear evidence of stimulated emission. From the above results and discussion, it is interpreted that THz emissions from graphene are stimulated by the coherent THz probe radiation and that the THz emissions are

amplified via photoelectron/hole recombination in the range of the negative dynamic conductivity.

Conclusion

In conclusion, we have successfully observed coherent amplified stimulated THz emissions arising from the fast relaxation and relatively slow recombination dynamics of photogenerated electrons/holes in an exfoliated graphene. The results provide evidence of the occurrence of negative dynamic conductivity, which can potentially be applied to a new type of THz laser.

Acknowledgement

This work was financially supported in part by the JST-CREST program, Japan, and a Grant-in-Aid for Basic Research (S) from the Japan Society for the Promotion of Science.

References

(1) Novoselov, K. S.; Geim, A. K.; Morozov, S. V.; Jiang, D.; Zhang, Y.; Dubonos, S. V.; Grigorieva, I. V.; Firsov, A. A. *Science* **2004**, *306*, 666–668.

(2) Katsnelson, M. I.; Novoselov, K. S. *Solid State Commun* **2007**, *143*, 3–13.

(3) Zhang, Y.; Tan, Y. W.; Stormer, H. L.; Kim, P. *Nature (London)* **2005**, *438*, 201–204.

(4) Novoselov, K. S.; Geim, A. K.; Morozov, S. V.; Jiang, D.; Katsnelson, M. I.; Dubonos, S. V.; Firsov, A. A. *Nature (London)* **2005**, *438*, 197–200.

(5) Katsnelson, M. I.; Novoselov, K. S.; Geim, A. K. *Nat. Phys.* **2006**, *2*, 620–625.

(6) Geim, A. K.; Novoselov, K. S. *Nat. Mater.* **2007**, *6*, 183–191.

(7) Ryzhii, V.; Ryzhii, M.; Otsuji, T. *J. Appl. Phys.* **2007**, *101*, 083114–083118.

(8) Dubinov, A. A.; Aleshkin, V. Y.; Ryzhii, M.; Otsuji, T.; Ryzhii, V. *Appl. Phys. Express* **2009**, *2*, 092301.

(9) V.Ryzhii,; Ryzhii, M.; Satou, A.; Otsuji, T.; Dubinov, A. A.; Aleshkin, V. Y. *J. Appl. Phys.* **2009**, *106*, 084507–084512.

(10) Dawlaty, J. M.; Shivaraman, S.; Chandrashekhar, M.; Rana, F.; Spencer, M. G. *Appl. Phys. Lett.* **2008**, *92*, 042116–042119.

(11) Sun, D.; Wu, Z. K.; Divin, C.; Li, X.; Berger, C.; de Heer, W. A.; First, P. N.; Norris, T. B. *Phys. Rev. Lett.* **2008**, *101*, 157402–157406.

(12) George, P. A.; Strait, J.; Dawlaty, J.; Shivaraman, S.; Chandrashekhar, M.; Rana, F.; Spencer, M. G. *Nano Lett.* **2008**, *8*, 4248–4251.

(13) Choi, H.; Borondics, F.; Siegel, D. A.; Zhou, S. Y.; Martin, M. C.; Lanzara, A.; Kaindl, R. A. *Appl. Phys. Lett.* **2009**, *94*, 172102–172105.

(14) Wang, H.; Strait, J. H.; George, P. A.; Shivaraman, S.; Shields, V. B.; Chandrashekhar, M.; Hwang, J.; Rana, F.; Spencer, M. G.; Ruiz-Vargas, C. S.; ; Park, J. *Appl. Phys. Lett.* **2010**, *96*, 081917 –081920.

(15) Kampfrath, T.; Perfetti, L.; Schapper, F.; Frischkorn, C.; Wolf, M. *Phys. Rev. Lett.* **2010**, *95*, 187403–187407.

(16) Breusing, M.; Ropers, C.; Elsaesser, T. *Phys. Rev. Lett.* **2009**, *102*, 086809–086813.

(17) Ando, T. *J. Phys. Soc. Jpn.* **2006**, *75*, 124701.

(18) Suzuura, H.; Ando, T. *J. Phys. Soc. Jpn.* **2008**, *77*, 044703.

(19) Rana, F.; George, P. A.; Strait, J. H.; Dawlaty, J.; Shivaraman, S.; Chandrashekhar, M.; Spencer, M. G. *Phys. Rev. B* **2009**, *79*, 115447–115452.

(20) Bonini, N.; Lazzeri, M.; Marzari, N.; Mauri, F. *Phys. Rev. Lett.* **2007**, *99*, 176802–176808.

(21) Rana, F. *Phys. Rev. B* **2007**, *76*, 155431–55436.

(22) Min, L.; Miller, R. J. D. *Appl. Phys. Lett.* **1990**, *56*, 524–526.